Analog Transmission for Space Very Long Baseline Interferometry

J. C. Springett[1]

Studies of advanced space very long baseline interferometry (SVLBI) missions envision data rates as high as 8 Gb/s, but to accomplish such high-rate data transfer from the spacecraft to ground using digital downlinks requires high effective isotropic radiated power (EIRP), as well as complex and substantially advanced modulation and receiving techniques. For these reasons, analog signal transfer becomes an attractive alternative. This article addresses the use of a technique dubbed constant envelope conversion (CEC) that permits analog VLBI signals to be efficiently transmitted using a saturated power amplifier. It is established that CEC analog transmission, compared to bandwidth compressive digital techniques such as M-quadrature amplitude modulation (QAM), requires no innovative designs and components to implement. CEC analog transfer is shown to provide VLBI fringe sensitivities no more than 0.5 dB less than those obtained from digital transmission, and for the same or much less spacecraft EIRP.

I. Introduction

Analog space very long baseline interferometry (SVLBI) signal transfer offers a viable alternative to sophisticated digital modulations. Its implementation does not require methods beyond the current state of the art. The RF bandwidth needed is essentially that of the VLBI observation bandwidth, while the downlink signal, using the constant envelope conversion (CEC) technique, employs the same transmitter saturated power amplifier as that used for digital transmission.

A. General Issues

Following the successful Tracking and Data Relay Satellite System (TDRSS) SVLBI demonstration in 1986, the use of an analog downlink was recommended during feasibility studies for the European Space Agency's (ESA's) Quasat mission (which was not funded). At that time, analog was preferred because it was believed that placing an entire multiple-mode RF-to-baseband converter on the spacecraft, complete with sampling and formatting, involved more complexity and power consumption than was warranted. These functions could more easily be accomplished on the ground using standard data terminals. Even so, a number of potential shortcomings of analog were recognized, but never analyzed in depth. They included the amplitude dynamics of the VLBI signal, effects of the propagation medium (ionosphere and troposphere), time synchronization, and calibration.

[1] NeoComm Systems, Inc., La Crescenta, California.

The research described in this publication was carried out by the Jet Propulsion Laboratory, California Institute of Technology, under a contract with the National Aeronautics and Space Administration.

The Japanese VLBI Space Observatory Program (VSOP) [or Highly Advanced Laboratory for Communications and Astronomy (HALCA)] SVLBI mission, operational (in the U.S.) from February 1997 to February 2002, made use of a single digital quadrature phase-shift-keyed (QPSK) VLBI data downlink (128 Mb/s on a 14.2-GHz carrier frequency). VSOP's initial development followed closely on the heels of Quasat in 1990, at a time when none of the realized drawbacks of analog SVLBI signal transfer had been satisfactorily resolved. As a result, mainly because the Japanese had already designed an acceptable analog-to-digital data converter and formatter for the spacecraft, and also since it was believed that downlink time transfer could be readily implemented for digital signals, VSOP embraced digital rather than analog signal transfer. Moreover, most of the ground digital receiving technology was already available by virtue of the various operational Earth resources satellite missions.

But as more advanced missions have been studied, such as Advanced Radio Interferometry between Space and Earth (ARISE), and SVLBI data rates as high as 8 Gb/s are contemplated, it has been quickly realized that digital downlinks will require some very complex, and extremely advanced (beyond the present state of the art), modulation and receiving techniques [1]. For these reasons, analog signal transfer again becomes an attractive approach and needs to be re-evaluated in light of fresh insights.

B. Analog SVLBI Transmission Overview

The VLBI signal has a Gaussian amplitude distribution (in the RF/IF domains or at the output of the baseband converter prior to quantization). Supposing downlink amplitude linearity must be preserved, this requires a spacecraft transmitter linear power amplifier, along with its relatively low efficiency (a situation akin to the use of digital 16-quadrature amplitude modulation (QAM) [1, Section V.A]). But there is an alternative. Since the ground terminal quantizes the VLBI signal to either one or two bits, it is necessary to provide linearity only to the extent that the two-bit quantization produces essentially the same result that would be obtained had no nonlinearity been introduced. Accordingly, the use of a technique, dubbed constant envelope conversion (CEC), that transforms the Gaussian dynamic into a phase-modulated sinusoidal waveform is envisioned. Analysis and simulations have shown that this technique can be made to work with only a few tenths of a dB loss with respect to the Gaussian waveform. Moreover, the use of CEC provides the spacecraft transmitter with a constant envelope input, so a more efficient saturated power amplifier can be employed.

The medium introduces signal degradations because of dispersion, delay fluctuations, scattering, and turbulence. Quasat was particularly concerned with the effects of the ionosphere because the downlink was to be at X-band (8.45 to 8.50 GHz). However, for Ka-band (37 to 38 GHz), only the consequences of the troposphere are significant. Of course, all ground radio telescopes also contend with the effects of the troposphere at the observing frequency. However, for the spacecraft radio telescope, it is not the observing frequency but the downlink frequency that counts. Thus, if the observing frequency is higher than the downlink frequency, the tropospheric degradation of the space radio telescope will be less than that for the ground radio telescope. Conversely, spacecraft observing frequencies less than the downlink frequency sustain more relative loss. However, the space radio telescope has a marked advantage in this regard over its ground counterpart because of the phase transfer link that uses judiciously placed pilot carriers, as well as cal-tones embedded in the analog data. The phase transfer link measures troposphere-induced phase fluctuations, while cal-tones gauge the frequency-selective effects of dispersion. It thereby becomes possible to largely correct for the tropospheric effects at the VLBI correlator.

VLBI signal-level calibration for an analog downlink is more difficult than for the digital downlink. Once digitized on the spacecraft, the VLBI data sent over a digital downlink are invariant to all subsequent transfer-related (especially amplitude) variations. By contrast, the analog downlink must contend with a continually changing path attenuation between the spacecraft and ground receiver. It therefore becomes necessary to provide appropriate automatic level control of the received analog signal up to the input to the ground analog-to-digital converter (ADC). This is expected to be readily accomplished by continual measurement and adjustment, based on a combination of the VLBI signal and pilot levels, prior to the ADC.

Time synchronization is a formidable task whether the downlink is analog or digital. The basic problem is to establish and maintain a precise epoch for the spacecraft observed signal with respect to ground time in the presence of Doppler and highly dynamic spacecraft-to-tracking station delays. For the VSOP digital link, the epoch is measured once each second as the time difference between the divided down data bit clock to 1 Hz and a local precision one-second time tick. But analog transmission does not directly allow this measurement. Alternatively, the aforementioned pilots not only provide the basis for a timing reference but also become the vehicle for VLBI-related telemetry information.

C. Specific Topics Addressed in this Article

The subsequent sections address the makeup of the complete analog system. In Section II, the elements of the complete analog system are specified in order to explain and emphasize the need for transmitting constant envelope analog signals in order to minimize signal distortion and link power requirements. Section III covers CEC theory and defines signal formats, investigates CEC spectra and signal-to-noise ratio (SNR) characteristics, and assesses radio telescope sensitivity loss using CEC. In Section IV, CEC implementation issues are outlined, including pilot-tone placement, spacecraft transmission and ground receiving circuits, time transfer, and troposphere phase correction. Finally, Section V outlines approaches for obtaining critical performance verification prior to committing the use of analog transmission to an actual SVLBI mission. This article, however, does not discuss the key topics of accomplishing signal-level control, the processing and use of cal-tones, or obtaining absolute time synchronization.

II. The Elements of a Complete Analog Link

The analog link has a strong affinity to the SVLBI digital link [1, Section III] in that it consists of simultaneous left circularly polarized (LCP) and right circularly polarized (RCP) components, plus pilot carriers for phase transfer, time synchronization, and telemetry. Figure 1 shows the generic block diagram. Within the spacecraft, the radio telescope downconverters are identical to those used for the digital link. C1 and C2 designate two independent signals[2] or channels. The radio telescope downconverters provide them at some low intermediate frequency (IF, 2–6 GHz). Constant envelope converters (one for each channel) contain the CEC processing (discussed below), the pilot combiners, and upconversion to RF (Ka-band). Following upconversion, the CEC channels are power amplified and transmitted to Earth, respectively, in LCP and RCP polarizations. At the ground receiving station,[3] the two channels are processed by a dual-polarization receiver, which tracks and demodulates the pilots and synthesizes frequency references for properly recovering and sampling the analog channels. Subsequent conversion from the analog to the digital domain (for recording) may be accomplished by adapting standard radio telescope data acquisition terminal (DAT) units.

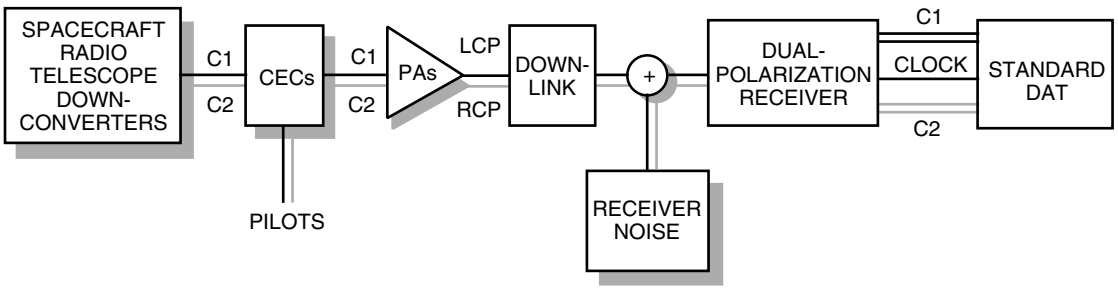

Fig. 1. High-level block diagram for an analog link.

[2] The use of the word "signal" in this article should be regarded as a generic term, used to stipulate any composite processes or waveforms, and not necessarily the radio telescope source or observation component alone.

[3] The station used to receive analog signals is essentially identical to that for digital signals as delineated in [2].

A. The Importance of Constant Envelope Conversion (CEC)

The characteristics of the analog circuits that pass the RF and IF signals are critical to the accuracy and sensitivity of the VLBI end-product visibility measurements. Generally, any signal mismatch between telescopes will degrade sensitivity or SNR. For example, filter passband amplitude and phase mismatches can become quite detrimental, and care is taken to limit losses due to their effects to less than 2.5 percent [3, Section 7.3]. Moreover, the power amplifiers (PAs) (shown in Fig. 3) induce types of signal distortion not found in ground radio telescopes, namely amplitude modulation-to-amplitude modulation (AM/AM) and amplitude modulation-to-phase modulation (AM/PM) conversions.

The employment of PAs involves the following paradoxical considerations. A PA is required to obtain a sufficient effective isotropic radiated power (EIRP) level for the analog channel so that the ground received signal-to-receiver-noise ratio is above some minimum number[4] (see Section II.C)). The highest output power and greatest efficiency is obtained when the PA is operated in its power saturation region. But this is also where the greatest degree of AM/AM and AM/PM conversion occurs. On the other hand, without a CEC unit before the PA, the amplitude of the bandpass signal input to the PA has a dynamic (Rayleigh) envelope. When the PA input is driven sufficiently hard to produce saturation (output compression) conditions over the majority of the input wave, consequential waveform amplitude and phase distortion result. This will now be illustrated.

B. Spacecraft Power Amplifier Distortion and Efficiency

Figure 2 shows the amplitude and phase transfer characteristics for a typical traveling-wave tube amplifier (TWTA) [4]. (The input and output voltage amplitudes are normalized to their corresponding values at saturation.) Solid-state power amplifiers exhibit similar performance. The input signal is a bandpass random process that may be represented by the standard quadrature and amplitude/phase mathematical forms:

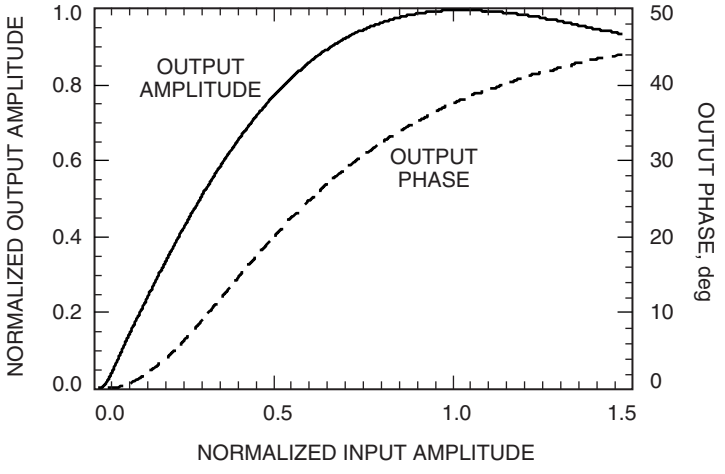

Fig. 2. Typical power amplifier transfer characteristics.

[4] This requirement is equivalent to maintaining a digital link bit error rate less than some maximum allowable value.

$$
\begin{aligned}
s_{\mathrm{RF}}(t) &= x(t)\cos[\omega_0 t] - y(t)\sin[\omega_0 t] \\
&= \sqrt{x^2(t)+y^2(t)}\cos\left[\omega_0 t + \tan^{-1}\left\{\frac{y(t)}{x(t)}\right\}\right] \\
&= a(t)\cos[\omega_0 t + \theta(t)] \qquad (1)
\end{aligned}
$$

where $x(t)$ and $y(t)$ are lowpass independent Gaussian noise voltages having single-sided lowpass rectangular bandwidth B Hz, and ω_0 is the center angular frequency. Figure 3 shows the result of passing $s_{\mathrm{RF}}(t)$ through the PA characteristics,[5] where the PA input drive level has been chosen to obtain the maximum output power. Distortion due to AM/AM and AM/PM conversion is plainly visible; large input peaks are suppressed and/or folded, and some zero crossings are displaced.

When CEC processing is interposed, a hard limiter eliminates the AM component $\sqrt{x^2(t)+y^2(t)}$ from Eq. (1). A fundamental-zone (around ω_0) bandpass filter (BPF)[6] follows the limiter, so the mathematical form into the PA becomes

$$
\begin{aligned}
cecs_{\mathrm{RF}}(t) &= \cos[\omega_0 t + \theta(t)] \\
&= \cos\left[\omega_0 t + \tan^{-1}\left\{\frac{y(t)}{x(t)}\right\}\right] \\
&= \frac{x(t)}{\sqrt{x^2(t)+y^2(t)}}\cos[\omega_0 t] - \frac{y(t)}{\sqrt{x^2(t)+y^2(t)}}\sin[\omega_0 t] \qquad (2)
\end{aligned}
$$

(The combination of a hard limiter followed by a zonal bandpass filter is customarily called a bandpass limiter.) Figure 4 shows the result of passing $cecs_{\mathrm{RF}}(t)$ through the PA characteristics, where again the PA input drive level has been set to obtain the maximum output power. Notice the nearly complete agreement between the input and output waveforms, showing that the effects of the AM/AM and AM/PM characteristics are essentially negligible.

The crucial point in favor of CEC is that CEC bandpass noise has a constant envelope property, much like digital QPSK. As a result, analog signal CEC effectively circumvents the PA nonlinearities, just as digital QPSK is unaffected by such transfer characteristics. This renders the transmitted signal very predictable, because it manifests only the CEC properties that are very stable. On the other hand, without CEC, the signal following the PA exhibits a degree of detrimental nonconformity. The consequence of this is illustrated by the following two measures obtained from the same simulation that produced Figs. 3 and 4. First, the ratio of Gaussian PA output power to CEC PA output power (both maximum) is 0.77 (-1.1 dB), which effectively represents a corresponding loss in link SNR. Secondly, and most importantly, the cross-correlation between the Gaussian PA output and the original Gaussian signal is a factor of 0.94 lower than the cross-correlation between the CEC PA output and the original Gaussian signal. This translates directly into a 6 percent loss of VLBI visibility.

---

[5] The waveforms shown were obtained using the simulation program SystemView. The PA input shown is the $x(t)$ lowpass component with a bandwidth of 256 MHz, and the PA output is the distorted $x(t)$ component obtained by coherently demodulating the PA output (and adjusting for delays).

[6] CEC theory and properties are detailed in Section III.

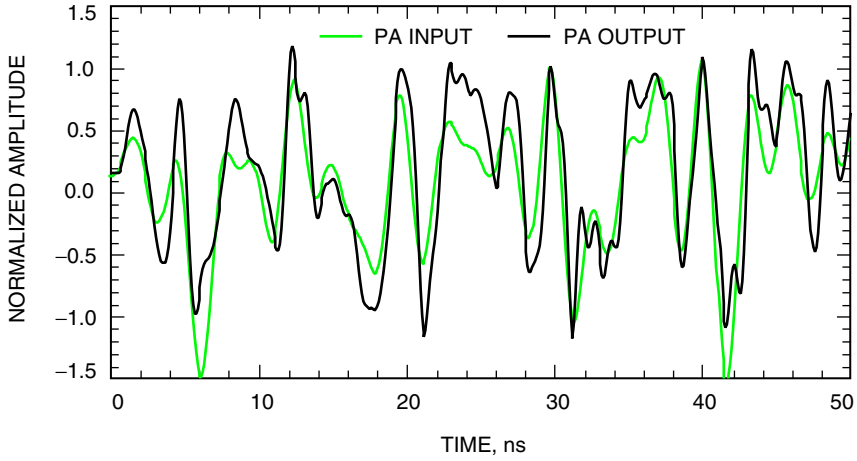

Fig. 3. PA input and output for a Gaussian quadrature-AM signal.

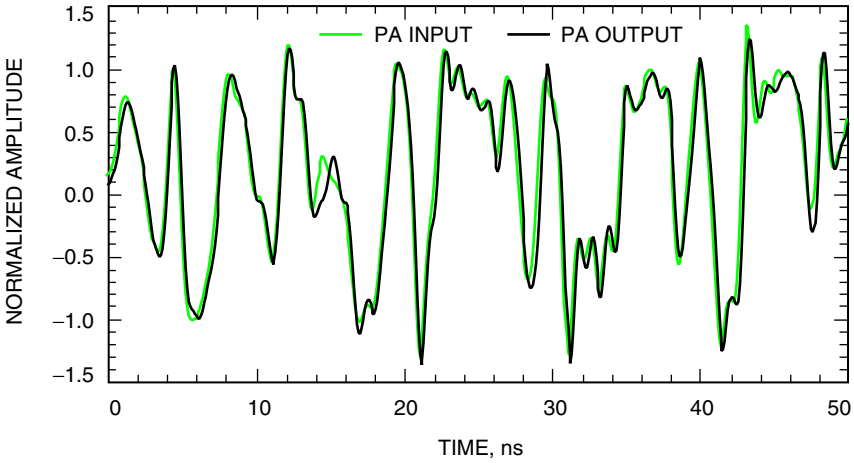

Fig. 4. PA input and output for a CEC quadrature-AM signal.

So, it should be clear that the use of CEC basically optimizes the analog link by not allowing power amplifier AM/AM and AM/PM nonlinearities themselves to measurably affect radio telescope performance. On the other hand, there is a fixed, but small, sensitivity loss (as defined in Section II.C and detailed in Section III.B) associated with the CEC process itself.

C. Link SNR Requirements

Prior to moving on to the CEC theory, the effects of downlink SNR on VLBI sensitivity are first considered. The observation-to-noise ratio (ONR) of the spacecraft telescope measurement prior to CEC is defined by

$$ONR = \frac{N_{\text{SOURCE}}}{N_{\text{RECEIVER}}} \tag{3}$$

while the ONR of the spacecraft telescope measurement following CEC becomes

$$ONR_{\text{CEC}} = \frac{N_{\text{SOURCE}}}{N_{\text{RECEIVER}} + N_{\text{CEC}}} = ONR \frac{N_{\text{RECEIVER}}}{N_{\text{RECEIVER}} + N_{\text{CEC}}} \tag{4}$$

where N_{SOURCE} is the observation received power at the output of the telescope receiver, N_{RECEIVER} is the noise contributed by the telescope receiver, and N_{CEC} is an effective noise added as a result of the CEC operation (see Section III.B). This assumes that all components may be treated as wideband and spectrally flat sources,[7] with the effective bandwidth of the CEC bandpass signal designated as $2B$. Following power amplification and transmission to Earth, additional noise, N_{GROUND}, is added by the ground receiver, so the downlink signal-to-noise ratio (SNR) is defined to be

$$SNR_{\mathrm{LINK}} = \frac{N_{\mathrm{SOURCE}} + N_{\mathrm{RECEIVER}} + N_{\mathrm{CEC}}}{N_{\mathrm{GROUND}}} \tag{5}$$

This treats the entire transmitted noise ensemble as the "signal" received by the ground station. The ground received ONR thus becomes

$$ONR_{\mathrm{GROUND}} = \frac{N_{\mathrm{SOURCE}}}{N_{\mathrm{RECEIVER}} + N_{\mathrm{CEC}} + N_{\mathrm{GROUND}}} = \frac{ONR_{\mathrm{CEC}} SNR_{\mathrm{LINK}}}{1 + ONR_{\mathrm{CEC}} + SNR_{\mathrm{LINK}}}$$

$$\cong ONR_{\mathrm{CEC}} \left(\frac{SNR_{\mathrm{LINK}}}{1 + SNR_{\mathrm{LINK}}} \right), \quad ONR_{\mathrm{CEC}} << 1, \quad SNR_{\mathrm{LINK}} >> 1 \tag{6}$$

The ratio enclosed by parentheses in Eq. (6) will be referred to as the link loss factor.

Now, the VLBI correlator sensitivity between the spacecraft observation and any ground radio telescope observation depends inversely on the standard deviation of the noise associated with the spacecraft observation and, therefore, will be a function of the square root of the link loss factor. The sensitivity loss factor due to downlink SNR accordingly becomes

$$\text{link sensitivity loss} = \sqrt{\frac{SNR_{\mathrm{LINK}}}{1 + SNR_{\mathrm{LINK}}}} \tag{7}$$

This is plotted in Fig. 5 as the percent of sensitivity loss versus downlink SNR.

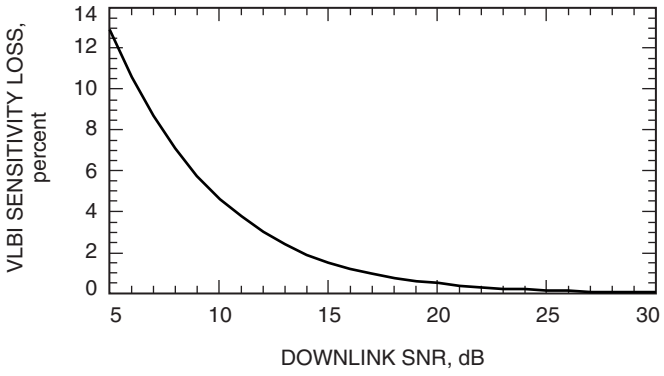

Fig. 5. VLBI sensitivity loss as a function of downlink SNR.

[7] Radio telescope sources considered in this article are treated as continuum radiation. The alternative of spectral line radiation, along with repercussions arising from the use of CEC, has not been assessed.

In [1, Section II], a case was made for digital SVLBI data transmission to the effect that the "maximum sensitivity loss is taken to be 2 percent, which corresponds to a received data $P_E^{MAX} = 1E-2$." Based upon this, and a statistical link performance methodology, a link budget for a 512-Mb/s channel was prepared [1, Table 3]. Given this result, but substituting analog CEC transmission for digital transmission, with all other relevant link parameters unchanged (including the transmitter power of 3.5 W), the question becomes: What is the comparable sensitivity loss? Table 1 provides the answer. Here, the nominal link margin of 10.8 dB, along with all other nominal parameters, has been reckoned to obtain the nominal downlink SNR in a $2B$ bandwidth of 128 MHz. (An analog bandwidth of 128 MHz corresponds to a digital bit rate of 512 Mb/s for Nyquist-rate 2-bit sampling.) This results in a nominal downlink SNR of 23.5 dB, while the no-margin (-3σ) downlink SNR becomes 12.7 dB. From Fig. 5, the downlink SNR of 12.7 dB results in a sensitivity loss of about 2 percent, the same as for the digital link. It therefore becomes possible to operate with either digital or analog CEC transmission using the same transmitter hardware and power to obtain comparable results.[8]

It is finally noted that since the downlink SNR depends directly on the ratio of transmitter power to VLBI RF bandwidth, i.e., $SNR_{\rm LINK} \propto P_T/B$, as B becomes larger, P_T needs only to increase proportionally. This is in striking contrast to the considerably more than proportionate P_T increases needed

Table 1. Link budget for 128-MHz analog signal transmission.

Ka-band analog downlink per polarization	Nominal value
Minimum downlink SNR (nominal SNR − link margin) (2 mm/h rain)	12.7 dB
Nominal downlink SNR (clear, humid)	23.5 dB
VLBI RF bandwidth (128 MHz)	81.1 dB-b/s
Available P_r/N_o	104.6 dB-Hz
Ground station 50 percent efficient 13.7-m antenna, uncooled LNA	
Ground station G/T_{sys}, 10-deg elevation angle	48.4 dB/K
Ground pointing loss	0.3 dB
Ground power received, P_r	−172.1 dBW
Propagation medium, 10-deg elevation angle	
Atmospheric loss (clear, humid)	1.9 dB
Propagation loss (max range= 36×10^3 km, 38.0 GHz)	215.1 dB
Polarization mismatch loss	0.2 dB
Spacecraft	
Provided spacecraft EIRP	45.1 dBW
Spacecraft pointing loss	0.3 dB
Spacecraft antenna gain (0.6-m dish)	45.5 dBi
Transmission circuit loss	5.5 dB
Provided spacecraft transmitter power	3.5 W
Provided spacecraft transmitter power	35.4 dBm
Nominal link margin	10.8 dB

[8] The analog link will undergo additional degradation due to troposphere phase corruption, but it is expected that this can be largely corrected, as discussed in Section IV.D.

by corresponding digital bandwidth compressing modulations [1, Sections IV.A and IV.B]. For example, with analog, if B increases by a factor of 3, then $3P_T = 3 \times 3.5$ W $= 10.5$ W. On the other hand, digital transmission (which goes from 512 Mb/s to 1536 Mb/s) requires a relatively enormous 160.0 W when employing 64-phase-shift-keying (PSK) modulation, or a "mere" 47.2-W peak for the more exotic 64-quadrature-amplitude-shift keying (QASK) modulation. Obviously, if transmitter power is the sole performance criterion, analog wins overwhelmingly.

III. Basic CEC Theory

The following subsections develop the form and characteristics of CEC signals. They begin by reviewing equivalent expressions for non-CEC in-phase (I) plus quadrature-phase (Q), and lower sideband (LSB) plus upper sideband (USB), models of the bandpass process. Also considered (for completeness) is the USB form of the entire signal. These same expressions are then extended to the CEC case. Following definitions, the topics of CEC spectra, demodulation, and sensitivity loss are explored.

A. CEC Signal I-and-Q and LSB-Plus-USB Forms

Equation (8) rewrites Eq. (1) in single-sideband (SSB) form and establishes $x(t)$ and $y(t)$ in terms of the

$$\begin{aligned} s_{\mathrm{RF}}(t) &= x(t)\cos[\omega_0 t] - y(t)\sin[\omega_0 t], && \text{(I \& Q)} \\ &= \frac{1}{\sqrt{2}}\left\{\lambda(t)\cos[\omega_0 t] + \hat{\lambda}(t)\sin[\omega_0 t]\right\} + \frac{1}{\sqrt{2}}\left\{\upsilon(t)\cos[\omega_0 t] - \hat{\upsilon}(t)\sin[\omega_0 t]\right\}, && \text{(LSB \& USB)} \\ &= \frac{1}{\sqrt{2}}\left\{\lambda(t) + \upsilon(t)\right\}\cos[\omega_0 t] - \frac{1}{\sqrt{2}}\left\{\hat{\upsilon}(t) - \hat{\lambda}(t)\right\}\sin[\omega_0 t], && \text{(I \& Q)} \end{aligned} \tag{8}$$

SSB components $\lambda(t)$ (lower sideband) and $\upsilon(t)$ (upper sideband). Like $x(t)$ and $y(t)$, $\lambda(t)$ and $\upsilon(t)$ are lowpass independent Gaussian noise voltages with rectangular bandwidth B Hz. The "$\hat{}$" over the variables denotes their Hilbert transform. Solving for the SSB components in terms of the double-sideband (DSB) components results in

$$\left.\begin{aligned} \lambda(t) &= \frac{1}{\sqrt{2}}\left\{x(t) + \hat{y}(t)\right\} \\ \upsilon(t) &= \frac{1}{\sqrt{2}}\left\{x(t) - \hat{y}(t)\right\} \end{aligned}\right\} \tag{9}$$

Another way of representing the bandpass signal is as the upper sideband of the carrier frequency $\omega_0 - 2\pi B$, which becomes

$$s_{\mathrm{USB}}(t) = z(t)\cos[(\omega_0 - 2\pi B)t] - \hat{z}(t)\sin[(\omega_0 - 2\pi B)t] \tag{10}$$

where $z(t)$ and $\hat{z}(t)$ are the Hilbert transform pair for a lowpass Gaussian noise voltage that has bandwidth $2B$ Hz; $z(t)$ and $\hat{z}(t)$ are related to the I and Q components by

$$\left.\begin{aligned} z\left(t\right) &= x\left(t\right)\cos\left[2\pi Bt\right] - y\left(t\right)\sin\left[2\pi Bt\right] \\ \hat{z}\left(t\right) &= x\left(t\right)\sin\left[2\pi Bt\right] + y\left(t\right)\cos\left[2\pi Bt\right] \end{aligned}\right\} \tag{11}$$

Turning next to the various CEC forms, Eq. (2) may be written in SSB form as

$$\begin{aligned} cecs_{\mathrm{RF}}\left(t\right) &= x_{\mathrm{CEC}}\left(t\right)\cos\left[\omega_0 t\right] - y_{\mathrm{CEC}}\left(t\right)\sin\left[\omega_0 t\right] \\ &= \frac{x\left(t\right)}{\sqrt{x^2\left(t\right)+y^2\left(t\right)}}\cos\left[\omega_0 t\right] - \frac{y\left(t\right)}{\sqrt{x^2\left(t\right)+y^2\left(t\right)}}\sin\left[\omega_0 t\right], \qquad \text{(I \& Q)} \\ &= \frac{1}{\sqrt{2}}\left\{\lambda_{\mathrm{CEC}}\left(t\right)\cos\left[\omega_0 t\right] + \hat{\lambda}_{\mathrm{CEC}}\left(t\right)\sin\left[\omega_0 t\right]\right\} \\ &\quad + \frac{1}{\sqrt{2}}\left\{\upsilon_{\mathrm{CEC}}\left(t\right)\cos\left[\omega_0 t\right] - \hat{\upsilon}_{\mathrm{CEC}}\left(t\right)\sin\left[\omega_0 t\right]\right\}, \qquad \text{(LSB \& USB)} \\ &= \frac{1}{\sqrt{2}}\left\{\lambda_{\mathrm{CEC}}\left(t\right)+\upsilon_{\mathrm{CEC}}\left(t\right)\right\}\cos\left[\omega_0 t\right] - \frac{1}{\sqrt{2}}\left\{\hat{\upsilon}_{\mathrm{CEC}}\left(t\right) - \hat{\lambda}_{\mathrm{CEC}}\left(t\right)\right\}\sin\left[\omega_0 t\right], \ \text{(I \& Q)} \end{aligned} \tag{12}$$

The CEC SSB components are given in terms of the CEC DSB components as

$$\left.\begin{aligned} \lambda_{\mathrm{CEC}}\left(t\right) &= \frac{1}{\sqrt{2}}\left\{\frac{x\left(t\right)}{\sqrt{x^2\left(t\right)+y^2\left(t\right)}} + \mathrm{H}\left[\frac{y\left(t\right)}{\sqrt{x^2\left(t\right)+y^2\left(t\right)}}\right]\right\} \\ \upsilon_{\mathrm{CEC}}\left(t\right) &= \frac{1}{\sqrt{2}}\left\{\frac{x\left(t\right)}{\sqrt{x^2\left(t\right)+y^2\left(t\right)}} - \mathrm{H}\left[\frac{y\left(t\right)}{\sqrt{x^2\left(t\right)+y^2\left(t\right)}}\right]\right\} \end{aligned}\right\} \tag{13}$$

where H[ ] indicates the Hilbert transform of the expression within the brackets.

The upper sideband expression of the carrier frequency $\omega_0 - 2\pi B$ is

$$cecs_{\mathrm{USB}}\left(t\right) = \frac{z\left(t\right)}{\sqrt{z^2\left(t\right)+\hat{z}^2\left(t\right)}}\cos\left[\left(\omega_0 - 2\pi B\right)t\right] - \frac{\hat{z}\left(t\right)}{\sqrt{z^2\left(t\right)+\hat{z}^2\left(t\right)}}\sin\left[\left(\omega_0 - 2\pi B\right)t\right] \tag{14}$$

with

$$\left.\begin{aligned} z_{\mathrm{CEC}}\left(t\right) &= \frac{z\left(t\right)}{\sqrt{z^2\left(t\right)+\hat{z}^2\left(t\right)}} = \frac{x\left(t\right)}{\sqrt{x^2\left(t\right)+y^2\left(t\right)}}\cos\left[2\pi Bt\right] - \frac{y\left(t\right)}{\sqrt{x^2\left(t\right)+y^2\left(t\right)}}\sin\left[2\pi Bt\right] \\ \hat{z}_{\mathrm{CEC}}\left(t\right) &= \frac{\hat{z}\left(t\right)}{\sqrt{z^2\left(t\right)+\hat{z}^2\left(t\right)}} = \frac{x\left(t\right)}{\sqrt{x^2\left(t\right)+y^2\left(t\right)}}\sin\left[2\pi Bt\right] + \frac{y\left(t\right)}{\sqrt{x^2\left(t\right)+y^2\left(t\right)}}\cos\left[2\pi Bt\right] \end{aligned}\right\} \tag{15}$$

On examination of the various CEC representations, it becomes apparent that the terms $x_{\mathrm{CEC}}(t) = x(t)/\sqrt{x^2(t)+y^2(t)}$ and $y_{\mathrm{CEC}}(t) = y(t)/\sqrt{x^2(t)+y^2(t)}$ govern the behavior of the CEC process, and therefore their properties will now be investigated.

B. CEC Spectra and SNR

In conformance with the SNR relationships given in Section II.C, let

$$\left.\begin{aligned} x\,(t) &= n_{\mathrm{Xsource}}\,(t) + n_{\mathrm{Xreceiver}}\,(t) \\ y\,(t) &= n_{\mathrm{Ysource}}\,(t) + n_{\mathrm{Yreceiver}}\,(t) \end{aligned}\right\} \tag{16}$$

with the additional conditions that $N_{\mathrm{SOURCE}} = \overline{n^2_{\mathrm{Xsource}}\,(t)} = \overline{n^2_{\mathrm{Ysource}}\,(t)}$ and $N_{\mathrm{RECEIVER}} = \overline{n^2_{\mathrm{Xreceiver}}\,(t)} = \overline{n^2_{\mathrm{Yreceiver}}\,(t)}$. Whether DSB or SSB demodulation of Eq. (8) is employed, yielding $x\,(t)$ and $y\,(t)$ or $\lambda\,(t)$ and $\upsilon\,(t)$, the ONR of each of these lowpass signals is given by Eq. (3). The lowpass ONR is in the strictly limited lowpass bandwidth 0 to B Hz (in other words, the spectrum is rectangular), and its corresponding normalized[9] autocorrelation function (inverse Fourier transform) becomes

$$r\,(\tau) = \frac{\sin\,[2\pi B\tau]}{2\pi B\tau} \tag{17}$$

For the CEC case, using Eqs. (1) and (2), the I and Q CEC terms are

$$\left.\begin{aligned} x_{\mathrm{CEC}}\,(t) &= \frac{x\,(t)}{\sqrt{x^2\,(t)+y^2\,(t)}} = \cos\left[\tan^{-1}\left\{\frac{y\,(t)}{x\,(t)}\right\}\right] = \cos\,[\theta\,(t)] \\ y_{\mathrm{CEC}}\,(t) &= \frac{y\,(t)}{\sqrt{x^2\,(t)+y^2\,(t)}} = \sin\left[\tan^{-1}\left\{\frac{y\,(t)}{x\,(t)}\right\}\right] = \sin\,[\theta\,(t)] \end{aligned}\right\} \tag{18}$$

Both $x_{\mathrm{CEC}}\,(t)$ and $y_{\mathrm{CEC}}\,(t)$ have the same normalized autocorrelation function, $r_{\mathrm{CEC}}\,(\tau)$, given by[10]

$$\begin{aligned} r_{\mathrm{CEC}}\,(\tau = t_2 - t_1) &= 2\overline{x_{\mathrm{CEC}}\,(t_1)\,x_{\mathrm{CEC}}\,(t_2)} = 2\overline{\cos\,[\theta\,(t_1)]\cos\,[\theta\,(t_2)]} = 2\overline{\cos\,[\theta_1]\cos\,[\theta_2]} \\ &= 2\int_{-\pi}^{\pi}\int_{-\pi}^{\pi}\cos\,[\theta_1]\cos\,[\theta_2]\,p\,[\theta_1,\theta_2;r\,(\tau)]d\theta_1 d\theta_2 \end{aligned} \tag{19}$$

where $p\,[\theta_1,\theta_2;r\,(\tau)]$ is the joint probability density function (PDF) of θ_1 and θ_2, and $r(\tau) = \overline{x_1 x_2}/\sigma_x^2$ (the normalized autocorrelation function of $x(t)$). This PDF may be found in [5, pp. 161–164, plus problem 10, p. 169]. The evaluation of the double integral is rather involved, so details are not provided (its assessment is facilitated by use of the computer program Mathematica). The result is

$$r_{\mathrm{CEC}}\,(\tau) = \frac{\mathrm{E}\,\left[r^2\,(\tau)\right] - \left(1 - r^2\,(\tau)\right)\mathrm{K}\,\left[r^2\,(\tau)\right]}{r\,(\tau)} \tag{20}$$

with $\mathrm{K}\,(m)$ and $\mathrm{E}\,(m)$ respectively being complete elliptic integrals[11] of the first and second kind.

---

[9] The value of normalized autocorrelation is unity for $\tau = 0$.

[10] The factor of 2 in Eq. (19) is the value that produces normalized autocorrelation unity for $\tau = 0$.

[11] $\mathrm{K}(m) = \int_0^{\pi/2}\left[1 - m\sin^2\varphi\right]^{-1/2}d\varphi$ and $\mathrm{E}(m) = \int_0^{\pi/2}\left[1 - m\sin^2\varphi\right]^{1/2}d\varphi$.

The CEC power density spectrum of $x_{\mathrm{CEC}}(t)$, based on the input rectangular spectrum for $x(t)$, is obtained by substituting Eq. (17) into Eq. (20) and performing the Fourier transform. This is accomplished numerically, with the result shown in Fig. 6. For this plot, $B = 1$, and the input and output spectrum powers (areas) are equal to unity. For the CEC spectrum, it may be seen that power is diverted from in-band ($B \leq 1$) to above-band ($B > 1$). The in-band power fraction is 0.90.

To determine the CEC output in-band ONR relative to the input ONR (assuming the $B > 1$ noise is discarded as part of the DAT processing), it is necessary to ascertain the amount of source signal present in $x_{\mathrm{CEC}}(t)$. Using the notation from Eq. (16), $x_{\mathrm{CEC}}(t)$ may be written as

$$x_{\mathrm{CEC}}(t) = \frac{n_{\mathrm{Xsource}}(t) + n_{\mathrm{Xreceiver}}(t)}{\sqrt{\left(n_{\mathrm{Xsource}}(t) + n_{\mathrm{Xreceiver}}(t)\right)^2 + y^2(t)}} \tag{21}$$

Here $n_{\mathrm{Xsource}}(t)$, $n_{\mathrm{Xreceiver}}(t)$, and $y(t)$ are all independent Gaussian variables. Expanding Eq. (21) as a power series in $n_{\mathrm{Xsource}}(t)$, the term involving the linear source component is

$$\text{series } n_{\mathrm{Xsource}}(t) \text{ term} = \frac{y^2(t)}{\left(n_{\mathrm{Xreceiver}}(t) + y^2(t)\right)^{3/2}} n_{\mathrm{Xsource}}(t) \tag{22}$$

So, the amount of source signal present in $x_{\mathrm{CEC}}(t)$ depends on calculating the expectation of $y^2(t)/\left(n^2_{\mathrm{Xreceiver}}(t) + y^2(t)\right)^{3/2}$. This cannot be done for arbitrary variables' standard deviations. Numerical evaluations therefore were performed for ONR values[12] of -10, -20, -30, and -40 dB, with respective results (termed α) of 0.620, 0.626, 0.627, and 0.627, when $\overline{x^2_{\mathrm{CEC}}(t)} = 0.5$. Note that α depends weakly on ONR. Designating the total noise component power of $x_{\mathrm{CEC}}(t)$ by η_{CEC}, it becomes (see footnote 9)

$$\eta_{\mathrm{CEC}} = 0.5 - \alpha^2 N_{\mathrm{SOURCE}} = 0.5 - \alpha^2\, ONR \tag{23}$$

Using Eq. (4), the in-band ONR thereby may be expressed as

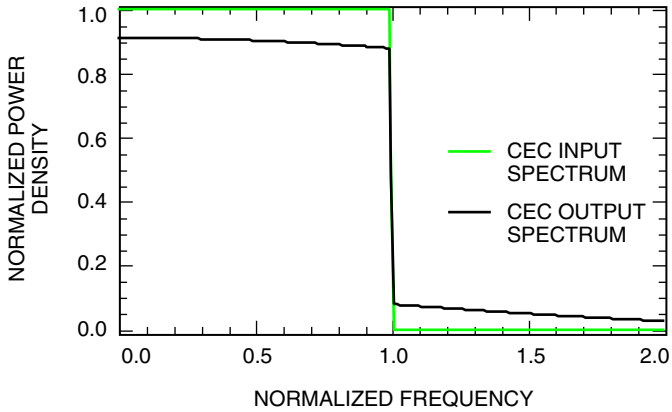

Fig. 6. CEC input and output spectra.

[12] When performing calculations, N_{RECEIVER} is conveniently set to unity, so that $ONR = N_{\mathrm{SOURCE}}$.

$$\text{in band } ONR_{\text{CEC}} = ONR \left\{ \frac{\alpha^2}{0.9\,(0.5 - \alpha^2\, ONR)} \right\} \tag{24}$$

The expression within the braces of Eq. (24) is the CEC ONR loss coefficient and is tabulated in Table 2. Lastly, the N_{CEC} term appearing in Eq. (4) may be solved for using Eq. (24), becoming (when $N_{\text{RECEIVER}} = 1.0$)

$$N_{\text{CEC}} = \frac{0.45}{\alpha^2} - 0.9\, ONR - 1 \tag{25}$$

Table 2. CEC ONR loss coefficient.

ONR, dB	α	CEC ONR loss, dB
−10	0.620	0.34
−20	0.626	0.57
−30	0.627	0.58
−40	0.627	0.59

C. Demodulation of CEC Signals

According to Eqs. (12) through (15), the CEC bandpass signal may be demodulated into lowpass components three ways: (1) as DSB components $x_{\text{CEC}}(t)$ and $y_{\text{CEC}}(t)$ that have baseband bandwidth B, (2) as LSB and USB components $\lambda_{\text{CEC}}(t)$ and $\upsilon_{\text{CEC}}(t)$ that also have bandwidth B, and (3) as a single USB component $z_{\text{CEC}}(t)$ having bandwidth $2B$.

It is common knowledge that, when $x(t)$ and $y(t)$ are lowpass independent Gaussian noise components in the bandpass noise process expressed by Eq. (1), the amplitude $a(t)$ has a Rayleigh probability density function (PDF), and the phase $\theta(t)$ is characterized by a uniform PDF over the range $-\pi \le \theta \le \pi$ [5, pp. 159–161]. Also well known (but seldom documented in noise theory texts) is that $cecs_{\text{RF}}(t)$ given by Eq. (2) has an amplitude PDF that is the same as that of a continuous sinusoid, namely [6, p. 39]

$$p\,(cecs_{\text{RF}}) = \begin{cases} \dfrac{1}{\pi\sqrt{1 - cecs_{\text{RF}}^2}} & |cecs_{\text{RF}}| \le 1 \\ 0 & |cecs_{\text{RF}}| > 1 \end{cases} \tag{26}$$

Now, Eq. (26) holds irrespective of any additional fixed-carrier phase offset ψ, and when $\omega_0 = 0$. As such, when $\psi = 0$, $cecs_{\text{RF}}(t) = x_{\text{CEC}}(t)$, or when $\psi = -\pi/2$, $cecs_{\text{RF}}(t) = y_{\text{CEC}}(t)$, and it may be readily concluded that both $x_{\text{CEC}}(t)$ and $y_{\text{CEC}}(t)$ have an amplitude PDF given by Eq. (26), i.e., they are essentially sinusoidal. Additionally, $z_{\text{CEC}}(t)$ is also sinusoidal because it has the same form as Eq. (2) with ω_0 replaced by $2\pi B$. So, in summary, the full-bandwidth (unfiltered) components $x_{\text{CEC}}(t)$, $y_{\text{CEC}}(t)$, and $z_{\text{CEC}}(t)$ all have sinusoidal amplitude PDFs akin to Eq. (26).

However, a small amount of lowpass filtering will drastically alter this characteristic. Consider the highly relevant case for $x_{\text{CEC}}(t)$ where the above-band ($B > 1$) spectral components of Fig. 6 are removed

by the dual-polarization receiver and DAT. The PDFs (obtained by simulation[13]) before and after filtering are shown in Fig. 7. Prior to filtering, the CEC PDF is that for a sinusoid with peak value ± 1.0, while the filtered CEC PDF takes on a somewhat trapezoidal shape, having a peak value of ± 1.6 and a standard deviation of 0.93. On the other hand, the SSB demodulated components $\lambda_{\mathrm{CEC}}(t)$ and $v_{\mathrm{CEC}}(t)$ involve more heavily filtered demodulation of the CEC bandpass signal, and their PDF appears rather Gaussian, as shown in Fig. 8. Here the peak values are ± 2.0, and the standard deviation is 1.16.

D. VLBI Correlation Sensitivity Loss due to CEC

As mentioned in Section II.C, the VLBI correlator sensitivity between the spacecraft observation and any ground radio telescope observation depends inversely on the standard deviation of the noise associated with the spacecraft observation. Therefore, the non-quantized sensitivity loss in dB due to the CEC process should amount to one-half of the CEC ONR loss factor given by Table 2 and is summarized in Table 3. Correlation here is between the spacecraft link that involves the CEC process and a ground radio telescope without CEC. The signals are also ideal, having rectangular spectra limited to B Hz.

On a more practical level, real filters will result in slightly poorer performance. Furthermore, the ideal case does not take into consideration 2-bit quantization of the signals prior to correlation. In order to get practical answers involving real filters and 2-bit quantization, it was necessary to resort to simulation, in which sufficiently precise results became very demanding in terms of computer processing time. For this reason, it was possible to simulate only an ONR of -10 dB, and the results for SSB demodulation are given in Table 4.

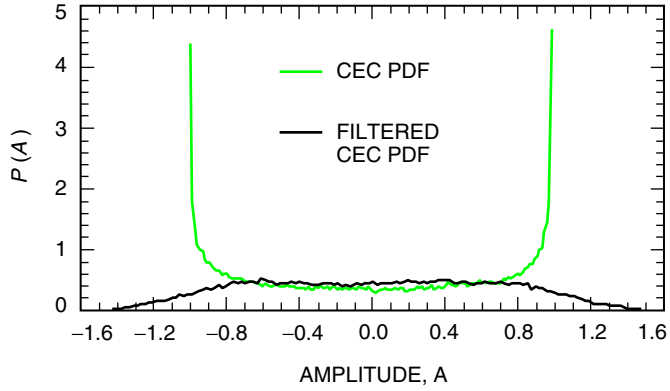

Fig. 7. CEC DSB $x_{cec}(t)$ unfiltered and filtered PDFs.

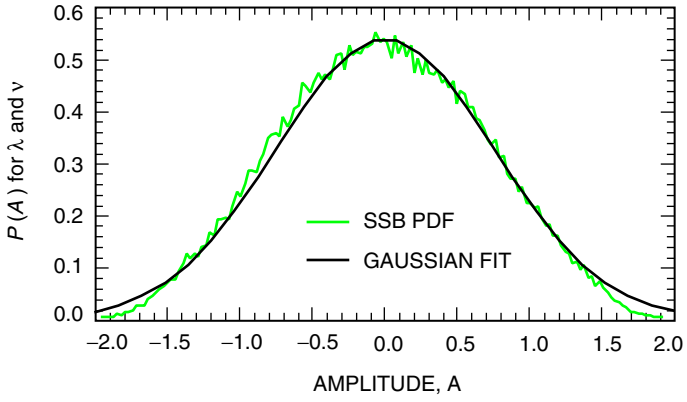

Fig. 8. CEC SSB $\upsilon_{cec}(t)$ PDF and Gaussian fit.

[13] Simulation data obtained in this article make use of the computer program SystemView.

Table 3. CEC correlation sensitivity loss.

ONR, dB	CEC sensitivity loss, dB
−10	0.170
−20	0.285
−30	0.290
−40	0.295

Table 4. Practical CEC SSB correlation sensitivity loss obtained from simulations.

ONR, dB	CEC theoretical no-quantization sensitivity loss, dB	CEC simulated no-quantization sensitivity loss, dB	CEC simulated 2-bit quantization sensitivity loss, dB
−10	0.17	0.25	0.27

For 2-bit quantization, the 4-level threshold voltages were placed at $\pm 0.9\sigma$ of the PDF shown in Fig. 8,[14] and the quantization weightings were set to ± 1 and ± 3. The small difference between the theoretical and simulated numbers may be attributed to practical rather than ideal elements, especially the filters. The important point is that the theoretical and simulated results pragmatically agree. Based on the values in Tables 3 and 4, it is conjectured that the practical CEC sensitivity loss for a lower ONR, say −30 dB, will not exceed 0.5 dB. This, however, is presently an unverified opinion.

IV. Implementation Issues

Obtaining the CEC sensitivity loss values outlined in Section III.D requires some special considerations regarding circuit implementation, as well as processing to minimize troposphere effects on the Ka-band downlink. These topics are addressed in the following four subsections.

A. CEC Spectra and Pilot Location

A design for the VLBI Space Observatory Program 2 (VSOP2) nominal digital data downlink rate of 1.024 Gb/s over the 37- to 38-GHz band is presented in [1, Section III]. Simultaneous LCP and RCP signals are used, with the data carrier frequencies offset by the symbol clock of 256 MHz and the pilots placed at the data spectra nulls (see Fig. 1 in [1]). The lowpass bandwidth corresponding to the four 2-bit quantized data streams d_{IL}, d_{QL}, d_{IR}, and d_{QR} is $B = 64$ MHz. For CEC transmission using simultaneous LCP and RCP signals, each RF band will effectively be $2B = 128$ MHz wide (which is one-forth the spectral null-to-null bandwidth of the digital spectrum).

Placement of the CEC bands and the pilots' locations within the 37- to 38-GHz allocation entails several possibilities that are illustrated by Fig. 9. In Fig. 9(a), the two RF bands (LHC and RHC) are both at mid-band ($f_0 = 37.5$ GHz), while the pilots are placed somewhat distant (near the edges of the 37- to 38-GHz range). This has the advantage that it requires the simplest ground dual-polarization

[14] Some limited experimentation with the threshold voltage was attempted. The results appeared to be fairly insensitive over the range of $\pm 0.8\sigma$ to $\pm 1.0\sigma$.

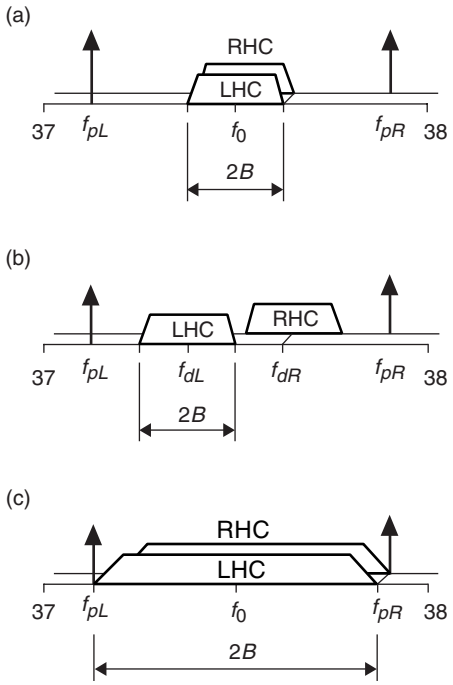

Fig. 9. Generic CEC spectra and pilot location candidates (not to scale): (a) mid-band overlapping narrow spectra, (b) offset non-overlapping narrow spectra, and (c) mid-band overlapping wide spectra.

receiver (see Section IV.C). A disadvantage is that using the same carrier frequency for each band subjects the CEC signals to cross-polarization degradation upon ground reception. To preclude this problem, the two bands may be offset in frequency as shown by Fig. 9(b). Although this is a good solution for the VSOP2 nominal system, one motivation for employing an analog link is that it becomes possible to obtain at least the equivalent of 7.168-Gb/s space radio telescope performance when $B = 448$ MHz.[15] In this case, $2B = 896$ MHz, the largest analog bandwidth that fills the 1-GHz-wide allocation while still being able to meet the National Telecommunications and Information Administration (NTIA) out-of-band emission regulations.[16] Of necessity, the two bands must completely overlap (again using $f_0 = 37.5$ GHz) as depicted by Fig. 9(c).

In general, the analog carrier and pilot frequencies may be specified by

$$\left.\begin{aligned} f_{dL} &= f_0 - \kappa B \\ f_{dR} &= f_0 + \kappa B \\ f_{pL} &= f_0 - \lambda B \\ f_{pR} &= f_0 + \lambda B \end{aligned}\right\} \tag{27}$$

[15] Candidate bandwidth increases above $B = 64$ MHz are sized in increments of 64 MHz.

[16] For a definition and discussion of NTIA regulations, see [1, Section III.A]. It seems likely that the output of the analog CEC transmitter should not require any high-order filtering to meet out-of-band requirements, as indicated in the final paragraph of Section IV.B below. However, the degree and effects of such filtering require further comprehensive analysis not possible during the current study.

where κ and λ are integers, or ratios of integers, and $f_0 = 37.5$ GHz (the center of the downlink band). For VSOP2, the use of analog CEC transmission (perhaps as an experiment or digital backup) should, if possible, make use of the same data carrier and pilot frequencies as the digital signals, which are $f_{pL} = 37.116$ GHz, $f_{dL} = 37.372$ GHz, $f_{dR} = 37.628$ GHz, and $f_{pR} = 37.884$ GHz. Table 5 summarizes the possibilities. "Spectra overlay" refers to the fact that the CEC in-band spectra in the LHC and RHC polarizations begin to extend beyond the center of the downlink band, so there is a partial cross-polarization spectral overlap. For $2B = 640$ MHz, even the pilot is overlapped by the CEC spectrum within the same polarization (see the discussion below about this). The cases of $2B = 768$ MHz and $2B = 896$ MHz cannot use the VSOP2 carrier frequencies stated above because the CEC in-band spectra will extend beyond the 37-GHz and 38-GHz band edges. These cases therefore must use $f_{dL} = f_{dR} = 37.500$ GHz.

Table 5. Analog possibilities for VSOP2 nominal carrier and pilot frequencies.

$2B$, MHz	Effective κ	Effective λ	Spectra overlay
128	2	6	No
256	1	3	No
384	2/3	2	Yes
512	1/2	3/2	Yes
640	2/5	6/5	Yes

In [1, Section III.B], a technique to combine the data and pilot carriers prior to joint carrier power amplification was addressed. This same method can be used for the CEC signals plus pilots with identical results. If the CEC signal power per polarization is 3.5 W (Section II.C above), then the pilot power will be 80 mW when the PA input pilot-to-CEC-signal power ratio is 0.40.

The digital data downlink has placed the pilots at the data spectrum nulls, and since the data spectrum power in the vicinity ($\pm$8 kHz) of the pilots is miniscule, the pilot-to-data-power-spectral-density ratio is essentially infinite; but this is not so for the analog pilots because the CEC signal spectrum has no nulls, as reference to Fig. 6 shows. Now, in most cases the pilots' frequencies will lie below or above the in-band spectral region, i.e., somewhere along the out-of-band spectrum tails. The worst-case situation is when the pilot is placed just above or below the in-band edge. For 3.5 W in the data spectrum, the data power spectral density at this point is about -87 dBW/Hz, and with a pilot power of 80 mW $= -11$ dBW, the pilot-to-data-power-spectral-density ratio is 76 dB-Hz. This is a very high value. As a point of comparison, the worst-case ground reception pilot-to-noise-power-spectral-density ratio (that results in acceptable pilot phase transfer and telemetry performance) is 62 dB-Hz. Even if the pilot were placed within the in-band spectral region (the $B \geq 320$-MHz cases), the pilot-to-data-power-spectral-density ratio will be no worse than 66 dB-Hz, which is still adequate. It therefore is concluded that CEC signal spectrum interference upon the pilot does not impose any limitations on pilot functional performance.

B. Spacecraft CEC Circuits

Figure 10 presents the functional block elements that make up a CEC. The signal arriving from the telescope receiver is provided at an IF ($f_{\rm IF}$) of a few GHz. In ground DATs (e.g., Mark III/IV), the input BPF filter is much wider than $2B$ to allow tuning to a desired sub-band. But for the spacecraft, the input BPF for the CEC process should be near $2B$, because if it is much wider than $2B$ a significant amount of the subsequent PA-supplied link power will be wasted. The simulation results reported at the end of Section III.D specified $2B$ as the -1-dB bandwidth of a 6-pole elliptic BPF providing an out-of-band rejection of -50 dB.

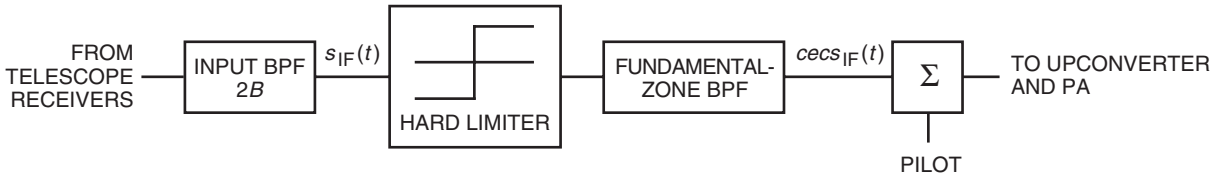

Fig. 10. CEC functional blocks.

The most critical circuit within the CEC is the limiter. It should be very wideband (at least 10 GHz), have a large dynamic range (reach the output limit over a 40-dB input level variation), provide excellent polarity symmetry (deviate from a 50 percent duty cycle by less than 2 percent for any test sine wave), and introduce minimal AM/PM conversion (no more than 5 deg). Generally, garden variety microwave limiters fall quite short of meeting these requirements (e.g., Mini-Circuits' PLS-2, which has an 800-MHz bandwidth and a 12-dB dynamic range). But a new class of GaAs metal semiconductor field effect transistor (MESFET)-limiting amplifiers, designed for post-reception data-stream conditioning on optical data links, have the desired qualities (e.g., OKI Electronic Components' KGL4217L; Sumitomo Electric's F0338915Q; Broadcom's BCM8118). However, none of these have actually been experimentally investigated for application to CEC, so whether they are able to perform as required is presently unknown.

Lastly, the output BPF is intended to pass the limiter's fundamental-zone spectral component and reject all higher zones. In theory, the fundamental zone (a mathematical abstraction) is infinite in extent over frequency and therefore overlaps all other harmonic zones. So the best that can be done is to pass as much of the spectrum around $f_{\rm IF}$ as possible while suppressing the harmonics. Simulation has shown that adequate performance is obtained for a Bessel 6-pole filter with a 3-db bandwidth of $6B$.

C. Ground CEC Receiver

Figure 11 is a block diagram of a receiver that derives demodulation references and sampling clock from the pilots and demodulates the wideband CEC carriers to an IF compatible with the DAT. The front-end block separates the two orthogonal polarization ensembles.[17] Each of the pilots, BPSK modulated by telemetry (nominally 8 kb/s), is recovered and filtered by means of Costas phase-locked loops (PLLs). Mixing the two pilot frequencies produces the sum frequency $2f_0$ and difference frequency $\lambda\,(2B)$, which are then respectively scaled by 1/2 to derive f_0 and $1/\lambda$ (see Section IV.A) to retrieve a frequency equal to $2B$. These are then processed by the carrier reference synthesizer, along with a locally generated frequency $f_{\rm IF}$, to obtain the references for translating the wideband CEC signals to the DAT's input frequency $f_{\rm IF}$. The DAT performs SSB demodulation of each signal and quantizes the lowpass results to 2 bits at a rate of $2B$ samples/second.

Doppler will shift all frequencies in the downlink signals, but the receiver functions to accommodate Doppler in a manner such that digital streams output from the DAT will have the same Doppler as if they were quantized on the spacecraft and transmitted as digital data. In other words, the subsequent VLBI correlation will use the same models whether the spacecraft downlink is digital or analog.

D. Time Transfer and Troposphere Phase Correction

For digital data downlinks, the time correction information needed by the VLBI correlator is obtained solely from a scaled form of the phase measured over the frequency transfer links between the phase transfer antenna[18] and spacecraft [7].[19] This is so because, once sampled and quantized on the spacecraft,

[17] Actually, the front-end block consists of all the RF-to-IF hardware shown in Fig. 2 of [2] up to the D/Cs located at the remote site; but, ignoring the fact that there will be downconversion from RF to some IF, the frequencies portrayed in Fig. 11 make use of the RF symbols from Fig. 9 in order to avoid introduction of additional nomenclature.

[18] This subsection assumes use of a segmented ground station that employs a large data antenna (DA) and a small phase transfer antenna (PTA). See [2] for concept and design details.

[19] R. D. Wietfeldt, *Time Corrections Generation for the DSN 11-m Network In Support of the VSOP and Radioastron Space VLBI Missions,* JPL D-17903 (internal document), Jet Propulsion Laboratory, Pasadena, California, October 13, 1998.

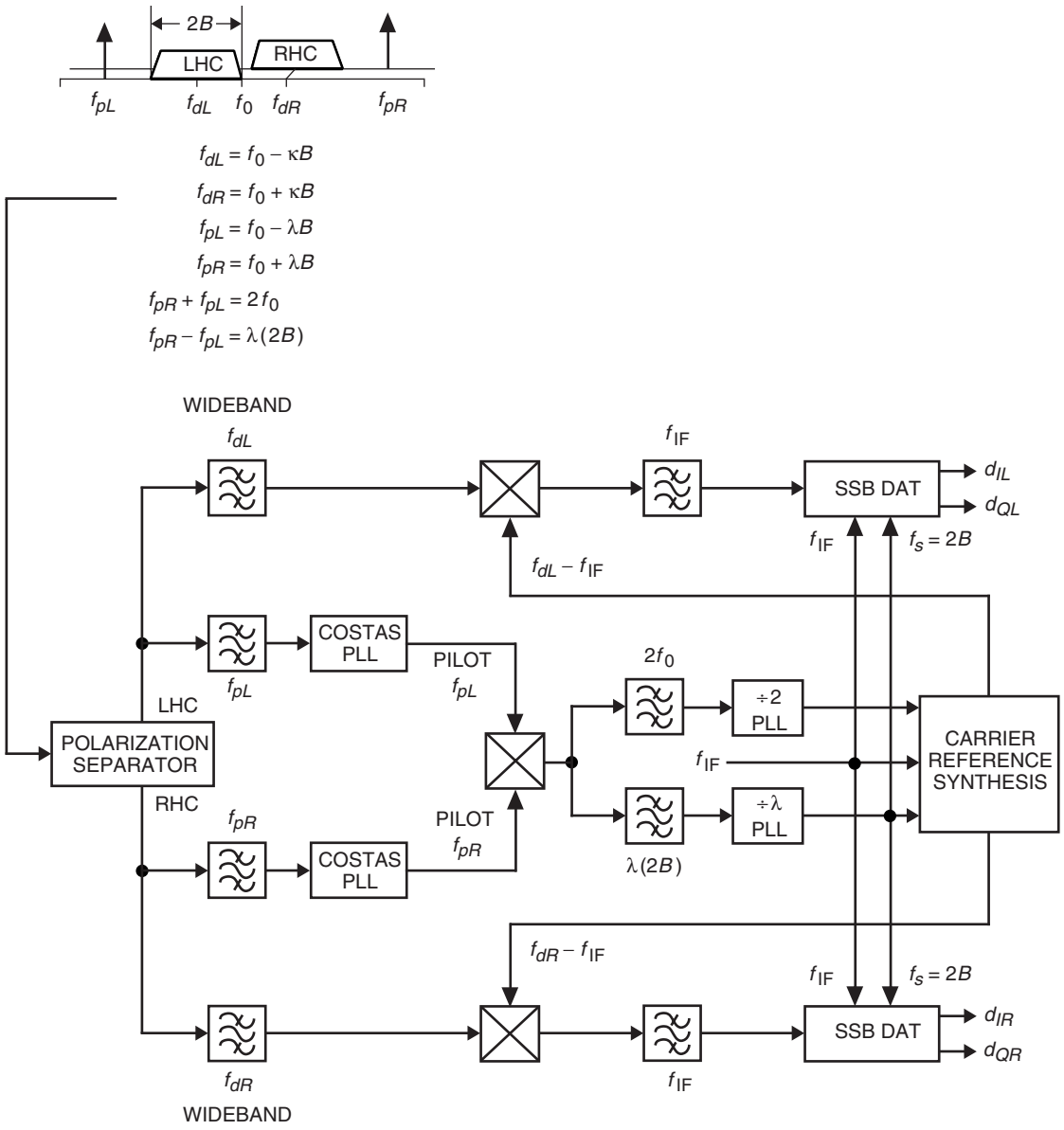

Fig. 11. Analog downlink dual-polarization LSB/USB receiver.

the VLBI data received on the ground are inherently insensitive to downlink perturbations, especially troposphere fluctuations.

Analog downlinks, on the other hand, will experience large phase undulations due principally to temporal variations of the wet component in the lower troposphere [3, Chapter 13]. The equivalent delay variation on the propagating downlink carriers can be as large as 3 cm,[20] which will introduce Ka-band phase changes of up to 1300 deg over spans of tens of minutes. Adequate corrections for such perturbations therefore must be made if analog VLBI signal transfer is to become a viable alternative to digital transmission.

[20] This number was provided by E. Fomalont, National Radio Astronomy Observatory.

The following briefly outlines an approach for measuring and scaling the information needed to perform time corrections (including the troposphere) for analog signal transmission. It must be noted that only rudimentary study of this critical topic has been accomplished, and a detailed analysis awaits additional sponsorship. Consequently, the subsequent discussion presents little more than a provisional assessment for processing the phase transfer metrics involving a segmented ground station architecture to obtain time (or phase) correction.

Figure 12 shows a highly simplified model for analog phase transfer in that it considers only one of the many induced phase transfer components,[21] namely the troposphere as represented by the blocks $\tau_1(t)$ and $\tau_2(t)$. The phase transfer antenna (PTA) and data antenna (DA) are assumed to be sufficiently separated so each points to the spacecraft (S/C) through different regions of the troposphere.

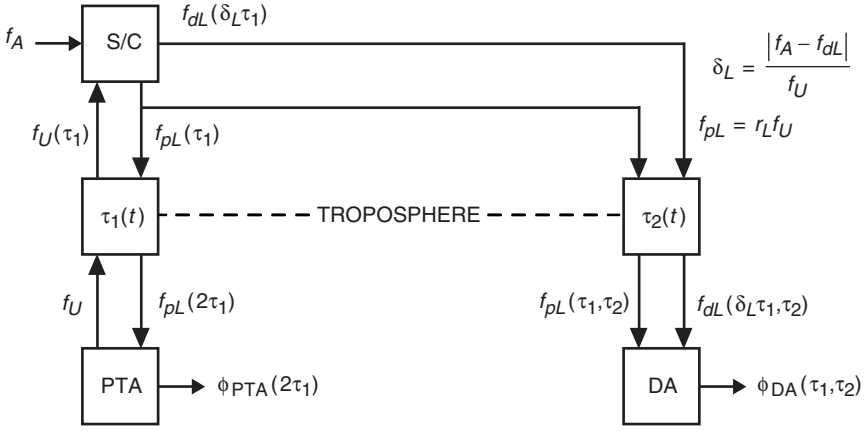

Fig. 12. Analog transmission phase-transfer model.

This explanation considers only use of the LHC pilot f_{pL} as the source for phase measurement information that may be used to correct troposphere perturbations of the analog signal on the LHC carrier f_{dL}. The PTA transmits f_U (nominally 40.2 GHz) through $\tau_1(t)$, becoming a function of the troposphere, denoted $f_U(\tau_1)$. Within the spacecraft, a PLL receives and tracks $f_U(\tau_1)$, and its output constitutes the basis for all frequencies and references used by the radio astronomy subsystem.[22]

The radio telescope source being observed arrives at frequency f_A and is translated to f_{dL} using the reference frequency $\delta_L f_U(\tau_1)$ (see Fig. 12 for the definition of δ_L). If $f_A > f_{dL}$, then the difference frequency (due to mixing) between f_A and the reference is taken and, when $f_A < f_{dL}$, the sum frequency is used. The translated radio telescope signal $f_{dL}(\delta_L\tau_1)$ effectively embodies $\delta_L\tau_1$ of the uplink troposphere, but upon transmission to the DA it is perturbed by $\tau_2(t)$, so the received signal becomes functionally $f_{dL}(\delta_L\tau_1, \tau_2)$.

The LHC pilot f_{pL} returning to the PTA passes through $\tau_1(t)$, and presuming complete reciprocity (a very good assumption), then the pilot arriving at the PTA is $f_{pL}(2\tau_1)$, and the phase measured by the Doppler processor within the PTA produces the measure $\phi_{\mathrm{PTA}}(2\tau_1)$. This same pilot returning to the DA passes through $\tau_2(t)$, so the pilot arriving at the DA is $f_{pL}(\tau_1, \tau_2)$, and the phase measured by a Doppler processor within the DA produces the measure $\phi_{\mathrm{DA}}(\tau_1, \tau_2)$.

The phase supplied to the correlator, based on the measured phases ϕ_{PTA} and ϕ_{DA}, that exactly corrects for the troposphere contributions to the analog radio telescope signal is

[21] See Table 1 in [7] for a comprehensive list.

[22] The uplink receiver scales f_U to a more standard frequency, such as 100 MHz, for use by the spacecraft frequency synthesis subsystem.

$$\phi_{\text{CORRECTION}} = \frac{\pm\,(f_A - f_{dL})}{2f_{pL}}\phi_{\text{PTA}} + \frac{f_{dL}}{f_{pL}}\phi_{\text{DA}} \tag{28}$$

where the "+" in "±" is taken when $f_A > f_{dL}$, and the "−" is taken when $f_A < f_{dL}$. The coefficients of ϕ_{PTA} and ϕ_{DA} in Eq. (28) are deemed scaling factors.

Now, as stated above, this result is an idealization that considers only the troposphere component among numerous induced phase transfer components. However, it equally applies to all components that are highly reciprocal, including the two-way Doppler residuals.[23] All of the non-reciprocal components arising from electronic circuits within the spacecraft and ground tracking station are relatively small by design and, therefore, are inconsequential regarding the essence of the scaling factors. Thus, Eq. (28) may be considered essentially optimum for the aggregate phase components.

It must be noted that measurement of ϕ_{DA} requires a Doppler processor at the DA, something not needed for digital data reception. In fact, a DA intended only for digital data reception has no strict frequency/phase stability requirements [2, Sections IV.A and V.C]. This changes for analog signal reception, where frequency referencing of the station's downconverters and phase measurement hardware must be derived from the local hydrogen maser frequency and time standard. Additionally, Doppler compensation must be supplied to the downconverters from which the received pilot phase is measured.

In closing this discussion, the reader is reminded that what has been presented is a tentative concept, and that the analysis and design of a complete receiving and time correction system (including absolute time synchronization) for both LHC and RHC signals has not been addressed.

V. CEC Performance Verification Possibilities

It is a fact that an SVLBI mission analog downlink has never been attempted and that the use of CEC in a radio telescope has never been tested. The results presented above, obtained from mathematical analysis and simulation, furnish a limited perspective on analog downlink performance. VSOP2 is the first mission that might make use of analog CEC transmission (perhaps as an experiment, if not as a means for obtaining significantly increased sensitivity). But well before such a commitment is made, first-hand experience with CEC and the challenge of troposphere phase correction is needed. The following two subsections offer some performance verification ideas.

A. Ground CEC Telescopes Experiment

Apart from the theoretical or simulated performance of CEC (Section III.D), there is always a practical value to be determined. Such an assessment may be obtained using two ground radio telescopes, as illustrated by Fig. 13, both observing the same strong source. For the reference telescope, everything is normal. But at the test telescope, the output of the IF is split into the data acquisition terminal (DAT), one path being normal and the other with a CEC circuit interposed. Within the DAT, one channel video converts and samples (two-bits) the normal signal, while another channel does the same for the CEC signal. Both formatted sample streams then are written to appropriate tape recorder tracks.

At the correlator, the tapes from the two telescopes are cross-correlated to produce fringes for the visibilities:

$$V_{\text{NORMAL}} = \langle S_{\text{REF}} * S_{\text{TEST}} \rangle_T \tag{29}$$

[23] Doppler residuals are the frequency errors arising from inexact predictive Doppler compensation used to remove most of the Doppler from the uplink and downlink pilots. These errors are typically less than 10 Hz, although they may occasionally rise to a level of a few hundred Hz.

and

$$V_{\mathrm{CEC}} = \langle S_{\mathrm{REF}} * S_{\mathrm{TEST-CEC}} \rangle_T \tag{30}$$

The "difference" between the SNR of these two results will be the degradation introduced by CEC.

If the experiment is conducted at Goldstone, the following possibilities exist. The observations may be done between DSS 13 and DSS 14, and the Real Time Block II correlator (RTB2) located at DSS 13 can provide fringes in real time, along with crude estimates of SNR. This will enable an ability to get things right before having the tapes processed at the correlator to obtain fringe fits and a good estimate of SNR.

Some restrictions will be imposed by the DSN Mark IV hardware, which has an IF distribution system that provides the two bandpass ranges of 96 to 224 MHz and 216 to 504 MHz. If the experiment is performed using 16-MHz baseband channels, then a CEC IF bandwidth of 32 MHz is needed. One mode for the experiment is to do exactly this by adding an additional BPF to the IF distribution output. Another mode is to use the 128-MHz and 288-MHz widths for the IF ranges stated above and simply rely on the post-demodulation LPFs within the DAT. Either mode should be capable of measuring the CEC sensitivity loss. But the disadvantage of not using a 32-MHz-wide IF is that the experiment cannot adequately assess the setting of the quantizer threshold for the quasi-Gaussian statistics of the 16-MHz SSB demodulated baseband signals following CEC from a 32-MHz IF (which is representative of the actual design for the spacecraft downlink).

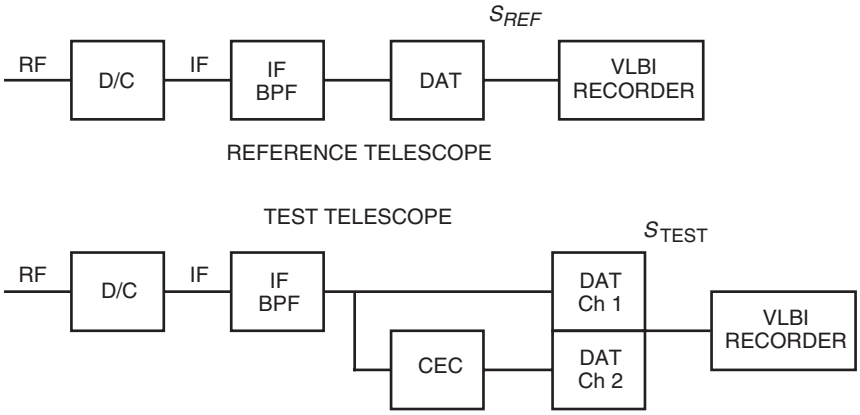

Fig. 13. Configuration for the CEC telescope experiment.

B. Phase Transfer and Troposphere Experiments

While the telescopes experiment just outlined should adequately test the performance of CEC itself, the critical phase transfer links are lacking. To test and verify phase transfer and time correction, some satellite emulation hardware is needed, along with the essential PTA and DA electronics. For satellite emulation, the radio telescope source signal may be realized using a pseudo-random noise generator. This has the advantage that an identical generator, along with some simple delay techniques, may be used in conjunction with a simple multiplication-averaging assembly to simulate the VLBI correlator. With such a setup, phase transfer can be evaluated in successively refined stages.

The first stage consists of an all-laboratory setup, where the troposphere-induced phase modulations and Doppler frequency residuals consist of generated functions ranging from sine waves to pseudo-arbitrary waveforms. These will permit unequivocal verification of all circuit operations and signal integrity. Even

before this hardware is constructed, the entire configuration may be designed and evaluated using computer simulation (e.g., SystemView and LabView). This first-stage effort (which includes the fabrication of the satellite emulator) is intended to flush out concept and design flaws.

A far more ambitious second stage is to make use of the hardware built during the first stage in conjunction with some actual Ka-band links through the troposphere. Clearly some type of PTA and DA is needed (but not necessarily those required for an actual spacecraft program). Since the troposphere of concern typically involves a scale height of 1 to 2 km, one way of performing the experiment is to place the satellite emulator atop a high mountain and locate the PTA and DA at a line-of-sight low elevation. The advantage of this setup is that the locations are all fixed (static), requiring the most minimal (and least expensive) PTA and DA. A disadvantage is there may be only a limited number of practical locations available.

A third stage (or second-stage alternative) might consist of placing the satellite emulator aboard a stratosphere balloon as a piggyback package to some primary mission. The National Scientific Balloon Facility (NSBF) located in Palestine, Texas (a NASA facility managed by the Physical Science Laboratory of New Mexico State University), provides the services of launching high-altitude (up to 36 km) research balloons, tracking them, and recovering the scientific experiments suspended beneath them. Each year approximately 16 launches are planned. Since tracking facilities are available, the need for providing complete PTA and DA facilities (especially the DA) might be lessened.[24] A disadvantage of the balloon test is that beneficial troposphere conditions may not happen during a "short" balloon flight time.

A fourth stage is to put the satellite emulator into Earth orbit as part of a research program or as a secondary payload to some other launch (such as SURFSAT-1 or the Shuttle/Space Station). This stage will require complete PTA and DA capabilities (hopefully a VLBI mission prototype station). A tremendous advantage to this approach is that, not only can the phase transfer links be extensively evaluated under real conditions, but additionally the satellite emulator serves to test the entire PTA and DA functions (including Doppler compensation and tracking).

VI. Summary and Conclusions

This article has presented rationale for utilizing analog SVLBI signal transfer, a viable and presumably lower-cost alternative to sophisticated digital modulations as means for providing equivalent data rates up to 4 Gb/s using the 37- to 38-GHz downlink band. Using a relatively simple technique, dubbed constant envelope conversion (CEC), to optimize spacecraft transmitter performance, analog transfer is shown to provide fringe sensitivities no more than 0.5 dB less than those obtained from digital transmission, and for the same or much less spacecraft EIRP. The lower cost of the analog method is predicated on avoiding the need to develop and implement complex state-of-the-art M-QAM transmission techniques for the spacecraft. Analog transmission, compared to M-QAM, requires no innovative designs and components to implement. The spacecraft implementation is uncomplicated, and the ground system requires no special data decoders. Although a unique ground receiver needed to track the pilot carriers and synthesize demodulation references requires development, VLBI signal channelization and digitization is accomplished within the tracking station using a standard data acquisition terminal (DAT).

Even though it might appear from this fervent summary that analog signal transfer is "the way," the reader should be aware that this article presents little more than an untested concept. For this reason, a number of performance verification options are offered, but they need additional funding for accomplishment. The reader is additionally reminded that, although this article is quite comprehensive, several important topics were not addressed. These include accomplishing signal level control within the

[24] Particulars concerning NSBF tracking capabilities have not been determined by the author. It is believed that the Wallops Flight Facility, and possibly White Sands facilities, may be involved.

ground receiver, the processing and use of cal-tones, a method for acquiring absolute time synchronization, and the effects of CEC on spectral line radiation-type sources. Each of these require further investigation before a complete and practical analog SVLBI link can be implemented.

References

[1] J. C. Springett, "Achieving Future Space Very Long Baseline Interferometry Gigabits-per-Second Data Rates," *The Interplanetary Network Progress Report 42-149, January–March 2002,* Jet Propulsion Laboratory, Pasadena, California, pp. 1–26, May 15, 2002.
http://ipnpr.jpl.nasa.gov/tmo/progress_report/42-149/149G.pdf

[2] J. C. Springett, "Space Very Long Baseline Interferometry Ground-Station Segmented Architecture," *The Interplanetary Network Progress Report 42-149, January–March 2002,* Jet Propulsion Laboratory, Pasadena, California, pp. 1–17, May 15, 2002.
http://ipnpr.jpl.nasa.gov/tmo/progress_report/42-149/149H.pdf

[3] A. R. Thompson, J. M. Moran, and G. W. Swenson, Jr., *Interferometry and Synthesis in Radio Astronomy,* Second Edition, New York: John Wiley & Sons, 2001 (First Edition 1986).

[4] A. A. M. Saleh, "Frequency-Independent and Frequency-Dependent Nonlinear Models for TWT Amplifiers," *IEEE Transactions on Communications,* vol. COM-29, no. 11, pp. 1715–1720, November 1981.

[5] W. B. Davenport, Jr., and W. L. Root, *An Introduction to the Theory of Random Signals and Noise,* New York: McGraw-Hill Book Company, 1958.

[6] D. Middleton, *An Introduction to Statistical Communication Theory,* York, Pennsylvania: McGraw-Hill Book Company, 1960.

[7] J. C. Springett, *Phase Stable Frequency Transfer for Orbiting VLBI Radio Telescopes,* NeoComm Systems, Inc., La Crescenta, California, October 15, 1992.